PAPER

Check for updates

Photodynamic therapy using hybrid nanoparticles comprising of upconversion nanoparticles and chlorin e6-bearing pullulan†

Riku Kawasaki, [ID] *‡ Takuro Eto,‡ Nanami Kono, Reo Ohdake, Keita Yamana, Hidetoshi Hirano, Shogo Kawamura, Naoki Tarutani, [ID] Kiyofumi Katagiri [ID] and Atsushi Ikeda [ID] *

With its minimal invasiveness, photodynamic therapy (PDT) is considered one of the most elegant modalities in cancer treatment. In this study, a facile hybrid nanoparticle was developed, composed of upconversion nanoparticles and chlorin e6-bearing pullulan, which can serve as a photosensitizer activated by a near-infrared red laser. Cell death induction in cancer cells was achieved through energy transfer from the near-infrared red laser emitted by the upconversion nanoparticles to chlorin e6. The therapeutic efficacy of our hybrid system surpassed that of the clinically available photosensitizer, Photofrin, and hybrid liposomes comprising upconversion nanoparticles and chlorin e6 were employed as control. Accumulation of our system in tumor tissue in tumor xenograft mice was primarily achieved through the enhanced permeability and retention (EPR) effect. The administered hybrids were excreted from each organ within 21 days after administration, minimizing the risk of undesirable side effects. Notably, our system exhibited 400 times higher PDT activity in tumor-bearing mice compared to the control groups. It also effectively inhibited metastasis.

Introduction

Despite the advancements in science, technology, and therapeutic modalities for cancer treatment, cancer remains the most lethal disease in many countries.[1,2] Furthermore, these therapies often come with severe side effects, highlighting the need to improve the quality of life of patients with cancer. In this regard, photodynamic therapy (PDT) is considered an elegant modality due to its minimal invasiveness, precise therapeutic efficacy, and *in situ* workability.[3] PDT involves the induction of cell destruction in cancer cells through the generation of cytotoxic reactive oxygen species by photosensitizers.[4–6] However, there are several challenges that need to be addressed to establish PDT as a sustainable therapeutic approach in cancer treatment.[7] First, the instability of photosensitizers in water can lead to their inactivation and the formation of undesirable aggregates.[8] Second, the poor absorbability of photosensitizers in the near-infrared red (NIR)

region, which can penetrate deeply into the body, poses a limitation.[9] Additionally, the selective delivery of photosensitizers to tumor tissues is currently inadequate, affecting therapeutic efficacy and potentially increasing side effects.[10] To fully utilize the potential of PDT in cancer treatment, the development of effective delivery platforms is crucial.

In this study, we have developed hybrid nanoparticles by combining a photosensitizer-bearing polysaccharide nanoparticle with upconversion nanoparticles (UCNPs) to create an NIR laser-activatable photosensitizer for PDT (Fig. 1).[11] Previously, we reported the successful development of chlorin e6-bearing pullulan (Che6P) nanoparticles, which improved the stability of chlorin e6 in aqueous media and demonstrated superior therapeutic efficacy compared to the commercially available photosensitizer, Photofrin.[12] These promising properties of Che6P nanoparticles as a photosensitizer motivated us to explore the potential of hybrid nanoparticles as an NIR laser-activatable photosensitizer for PDT. To enhance the light absorbability of Che6P nanoparticles in the NIR region and enable efficient activation in biological systems, we focused on UCNPs,[13] which can convert NIR light into visible light.

This study focuses on evaluating the performance of hybrid nanoparticles, Che6P-UCNPs, as an NIR laser-activatable photosensitizer in cancer therapy. Che6P-UCNPs could convert dissolved oxygen into cytotoxic singlet oxygen through energy

Program of Applied Chemistry, Graduate School of Advanced Science and Engineering, Hiroshima University, 1-4-1 Kagamiyama, Higashi Hiroshima, 739-8527, Japan. E-mail: riku0528@hiroshima-u.ac.jp, aikeda@hiroshima-u.ac.jp
†Electronic supplementary information (ESI) available: Experimental procedure and analytical data. See DOI: https://doi.org/10.1039/d4bm00769g
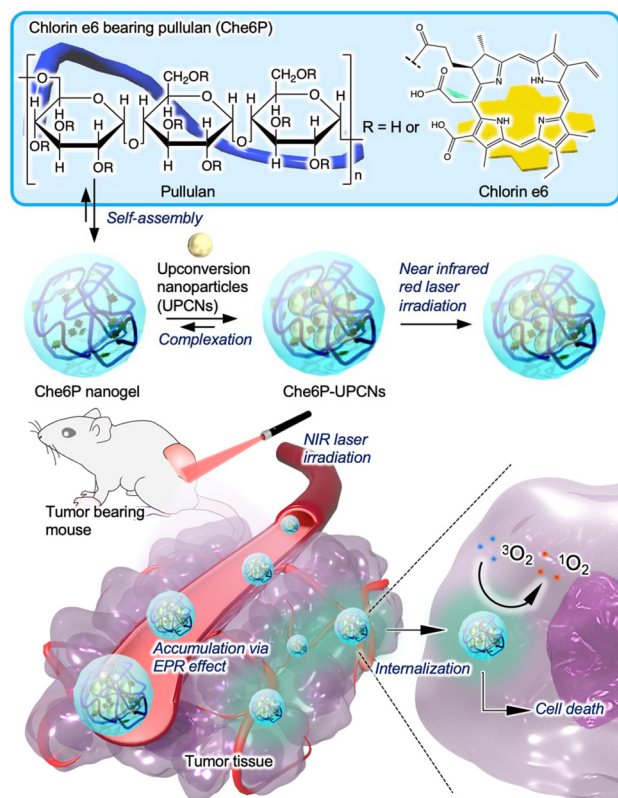‡These authors contributed equally to this work.

Fig. 1 Schematic illustration of photodynamic activity against cancer spheroid using hybrid nanoparticle comprising upconversion nanoparticles and chlorin e6-bearing pullulan.

transfer from NIR laser emitted UCNPs to chlorin e6 molecules in aqueous media. Che6P-UCNPs induced cell destruction upon NIR laser irradiation, and their therapeutic efficacy surpassed that of Photofrin and hybrid liposomes comprising Che6 and UCNPs. Additionally, results from the spheroid growth inhibition assay indicated the potential applicability of our system as a photosensitizer in cancer treatment. Furthermore, the intravenous injection of Che6P-UCNPs resulted in sufficient tumor tissue accumulation. Notably, the hybrid nanosystems were effectively cleared from major organs, such as the liver and spleen, mitigating the risk of undesirable side effects. *In vivo* experiments using a tumor xenograft model further confirmed the performance of the hybrid nanosystem as an NIR-activatable photosensitizer. Treatment with Che6P-UCNPs under NIR irradiation successfully suppressed tumor growth and significantly inhibited tumor metastasis, a crucial aspect in cancer treatment.

Results and discussion

Preparation of hybrid nanoparticles comprising of UCNPs and chlorin e6 bearing pullulan

Che6P was synthesized, as previously described (Scheme S1†).[12] The effects of the substitution degree of

chlorin e6 molecules on the physicochemical properties of the hybrid nanoparticles and the therapeutic efficacy of PDT were investigated. The substitution degree of chlorin e6 to glucose units of the polymers was quantified as 0.54, 2.22, and 2.80, respectively, using UV–Vis absorption spectroscopy (Fig. S1,† solid line) and ^{1}H NMR (Fig. S2†). The resulting Che6P molecules were labeled as Che6P-0.54, Che6P-2.22, and Che6P-2.80, respectively.

The nanoparticles were prepared as previously described.[12] The hydrodynamic diameter (D_{hy}) of Che6P-0.54, Che6P-2.22, and Che6P-2.80 was 227, 153, and 128 nm, respectively, based on dynamic light scattering (DLS) (Table 1). These measurements indicated that the hydrophobized polysaccharide formed small nanoparticles by packing the substituted chlorin e6 molecules within each nanoparticle. Furthermore, the nanoparticle size remained relatively stable for two days, suggesting colloidal stability in aqueous media (Fig. S3†). ζ-Potential measurements revealed the negatively charged nature of the Che6P nanoparticles. Transmission electron microscopy (TEM) observations confirmed the spherical morphology of the Che6P nanogels (Fig. S4†), with sizes consistent with the results obtained by DLS. Additionally, the absorption spectra of chlorin e6 molecules broadened (Fig. S1,† dashed line), and the fluorescence from chlorin e6 was quenched (Fig. S5†) after formulation, suggesting the systems were formed *via* self-aggregation of chlorin e6.

In this work, oleic acid-capped Er/NaYF$_4$:Yb was used as UCNPs since it can convert NIR to green light (Fig. 2a purple and S6†), which is suitable for chlorin e6 activation due to spectral matching. The D_{hy} of UCNPs was around 20 nm, and TEM observation revealed spherical morphology with a 20 nm diameter (Fig. 2b). Che6P-UCNPs were prepared using the injection method based on supramolecular chemistry.[14,15] UCNPs dispersed in tetrahydrofuran at concentrations of 1, 10, and 100 μg mL^{-1}; (500 μL) were injected into an aqueous dispersion of Che6P nanoparticles (0.1 mg mL^{-1}, 10 mL). Hybrid nanoparticles were spontaneously formed, primarily through hydrophobic interactions. The resulting dispersion appeared homogeneous and transparent, indicating the encapsulation of UCNPs by Che6P nanoparticles.

The D_{hy} value of the Che6P nanoparticles did not significantly change upon complexation with UCNPs (Table 1). The sizes obtained were suitable for achieving the enhanced permeability and retention (EPR) effect, which is crucial for passive tumor targeting properties.[16] The electrically anionic character of Che6P nanogels, resulting from the presence of free carboxylic acid in chlorin e6, also shifted to electrically neutral (-0.1–1 mV), suggesting that chlorin e6 molecules were anchored in the hydrophobic layer on the UCNP surface, while the UCNPs were surrounded by the electrically neutral polymer backbone of pullulan. TEM observation without staining revealed the cluster-like structure of UCNPs (Fig. 2c, d, e, and S7†). The number of UCNPs increased with the UCNPs concentration (Table S1†).

After complexation, the absorption spectra of Che6P nanoparticles broadened (Fig. S8†), indicating that the flexibility of

Table 1 Basic characterization of Che6P-UCNPs

	[Che6P]/μg mL^{-1}	UCNPs/μg mL^{-1}	D_{hy}^{a}/nm	PDI^a	ζ-Potential^b/mV	$^1O_2$ conversion rate^c/fmol min^{-1}
UCNPs	—	—	22 ± 0.1	0.18	—	—
Che6P-0.54	100	0	243 ± 8	0.18	−4.1 ± 8	10 ± 5
Che6P-0.54-UCNPs-1	100	1	282 ± 5	0.19	−1.0 ± 0.4	87 ± 7
Che6P-0.54-UCNPs-10	100	10	242 ± 8	0.22	−1.4 ± 0.3	47 ± 3
Che6P-0.54-UCNPs-100	100	100	243 ± 11	0.26	−0.4 ± 0.7	555 ± 73
Che6P-2.22	100	0	212 ± 8	0.24	−15 ± 1	143 ± 6
Che6P-2.22-UCNPs-1	100	1	214 ± 20	0.23	−3.8 ± 1	106 ± 12
Che6P-2.22-UCNPs-10	100	10	218 ± 6	0.26	−1.5 ± 0.1	138 ± 5
Che6P-2.22-UCNPs-100	100	100	242 ± 7	0.25	−0.2 ± 0.1	161 ± 15
Che6P-2.80	100	0	145 ± 3	0.19	−13 ± 0.1	99 ± 5
Che6P-2.80-UCNPs-1	100	1	119 ± 1	0.18	−0.1 ± 0.1	22 ± 4
Che6P-2.80-UCNPs-10	100	10	167 ± 14	0.13	−0.1 ± 0.1	9 ± 6
Che6P-2.80-UCNPs-100	100	100	206 ± 2	0.24	−0.1 ± 0.1	73 ± 3
Hybrid liposome	100	100	120 ± 1	0.15	−0.7 ± 0.1	61.5 ± 8

^{a} Hydrodynamic diameter (D_{hy}) of UCNPs, Che6P nanogel, and Che6P-UCNPs was measured using Zetasizer Nano ZS. UCNPs were dispersed in tetrahydrofuran. Che6P nanogel and Che6P-UCNPs were dispersed in MilliQ (pH, 7.4; 25 °C). PDI value was calculated by cumulant methods. ^{b} ζ-Potential was measured by using the capillary cell. ^{c} Singlet oxygen ($^1O_2$) conversion rate was calculated by initial slope in consuming ABDA.
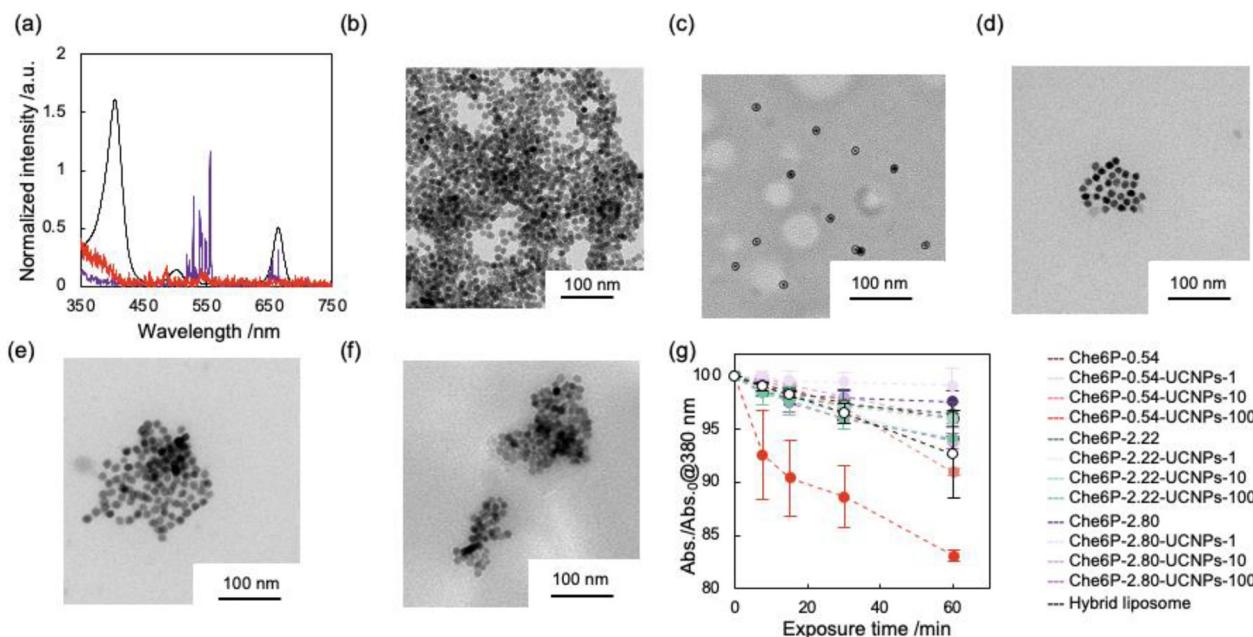

Fig. 2 Characterization of Che6P-UCNPs. (a) Comparison of UCNPs emission spectra between UCNPs (purple) and Che6P-UCNPs (red). Black line indicates the absorption spectrum of Che6P-0.54. (b) Representative morphology of UCNPs. The samples were observed using TEM without staining. Accelerate voltage was set at 100 kV. (c, d and e) Representative morphology of Che6P-0.54-UCNPs-1 (c), Che6P-0.54-UCNPs-10 (d), and Che6P-0.54-UCNPs-100 (e). The samples were observed using TEM without staining. Accelerate voltage was set at 100 kV. (f) Representative morphological images of hybrid liposomes. The samples were observed using TEM without staining. Accelerate voltage was set at 100 kV. (g) Time course of 9,10-anthracenediyl-bis(methylene) dimalonic acid (ABDA) bleaching through oxidation by $^1O_2$ data represented as mean ± Standard deviation (n = 3).

the chlorin e6 moiety was reduced by insertion into the alkyl chain of oleic acid on the surface of UCNPs. The fluorescence from chlorin e6 also slightly increased upon complexation (Fig. S9†), suggesting that the anchoring of chlorin e6 into oleic acid helped moderate the self-aggregation of chlorin e6 molecules. Furthermore, the fluorescence from UCNPs around 520–550 nm and 640–660 nm in Che6P-UCNPs (Fig. 2a, red) overlapped with the absorption of chlorin e6,

indicating an efficient energy transfer between UCNPs and chlorin e6 when the UCNPs were activated by a 980 nm laser.

In this work, we employed hybrid liposomes comprising UCNPs and Che6 as NIR laser irradiation activatable control using conventional DDS carrier. The hybrid liposomes were prepared *via* extrusion methods (DOPC, 10 mM; UCNPs, 100 μg mL^{-1}; Che6, 33.1 μM).[17] The D_{hy} of hybrid liposomes were determined to be 120 nm and the agglomerate of UCNPs

was observed by TEM (Fig. 2f), indicating these nanoparticles not located within lipid bilayer but coated with lipid membrane.

The ability of Che6P-UCNPs to generate singlet oxygen under laser irradiation was evaluated using an anthracene derivative (ABDA) as a probe (Scheme S2†)[18] and their conversion efficiency was compared with hybrid liposomes. The absorption of ABDA (350–400 nm) was bleached over time due to oxidation by singlet oxygen generated by Che6P-UCNPs under NIR laser irradiation (Fig. S10†). In the absence of UCNPs, Che6P nanoparticles alone could not convert dissolved oxygen into singlet oxygen over a 1 h period of NIR laser irradiation (Fig. 2g, dashed line). However, in the presence of Che6P-UCNPs, a decrease in ABDA absorbance was observed upon laser exposure, and the amount of singlet oxygen generated increased with the concentration of UCNPs in all systems (Fig. 2g, solid line). For example, in the case of Che6P-0.54-UCNPs-100, 16% of ABDA was consumed after 60 min of irradiation. These results indicate that the upconverted red emission from UCNPs effectively activated the chlorin e6 in the Che6P molecules through NIR laser irradiation. Additionally, the Che6P-0.54-UCNPs-100 system exhibited the highest efficiency among the Che6P-UCNPs systems (Table 1). As the substitution degree of chlorin e6 increased, the conversion efficiency of ABDA decreased, suggesting that a larger amount of chlorin e6 molecules could induce undesirable self-quenching through molecular packing within the polymer matrix of each hybrid nanoparticle. Though the loaded amount of UCNPs and Che6 in hybrid liposomes are same as Che6P-0.54-UCNPs-100, photodynamic activity of our hybrid nanogel system was 9 times higher than that of hybrid liposomes under NIR laser irradiation. We hypothesized that the differences in $^1O_2$ generation capacity between Che6P-0.54-UCNPs-100 and hybrid liposomes was caused by accessibility of dissolved oxygen to photo-activated chlorin e6. In case of hybrid liposomes, chlorin e6 located in lipid membrane which shield access of dissolved oxygen to chlorin e6, resulting in $^1O_2$ generation efficiency got lessened. In addition, the difficulty in control of distance between UCNPs and Che6 molecules, which is important to achieve efficient energy transfer, could decrease the conversion efficiency. In contrast, dissolved oxygen can easily access to the chlorin e6 since the large part of nanogel in volume was occupied with water and chlorin e6 should be surrounded by polysaccharides which can be easily hydrated. These fascinating properties of Che6P-0.54-UCNPs can potentially enhance photodynamic activity of chlorin e6. Importantly, during this period, more than 98% of the absorbance of chlorin e6 remained in all systems (Fig. S11†), and no undesirable precipitation was observed, indicating the stability of the current systems under photo-irradiation.

Photodynamic activity of hybrid nanoparticles *in vitro*

To assess the biocompatibility of the current system as a photosensitizer, its effect on murine fibroblast cells (L929), which serve as a healthy cell model, was evaluated in dark con-

dition by WST-8 assay. No significant cytotoxicity was observed in any of the systems, indicating that the hybrid systems are non-cytotoxic and suitable as photosensitizers (Fig. S12†). In the current conditions, NIR laser irradiation resulted in no L929 cell destruction (Fig. S13†), suggesting that our system can avoid severe side effects on healthy tissues.

The performance of Che6P-UCNPs as a photosensitizer was compared to that of Photofrin and hybrid liposomes,[19] which was used as a control. Photofrin and hybrid liposomes did not induce cytotoxicity even under NIR laser irradiation (Fig. 3a, dashed line, yellow and white symbols). In contrast, photo-induced cytotoxicity was observed only when Colon26 cells were exposed to Che6P-0.54-UCNPs-100 for 24 h (Fig. 3a, solid line, red symbols, S14, and S15†). The order of photodynamic activity *in vitro* was comparable to singlet oxygen generation capacity (Fig. S16†). The half-maximal inhibitory concentration (IC_{50}) value was estimated to be 0.22 μM. The photodynamic activity against cancer cells is comparable to the capability of Che6P-UCNPs to generate singlet oxygen. We further addressed mechanism in cell death using Che6P-0.54-UCNPs-100 under NIR-laser irradiation by Annexin V-PI method.[20] When the cells treated with Che6P-0.54-UCNPs-100 without exposure of NIR-laser, the population of the cells were similar to that of non-treated cells (Fig. S17†). In contrast, the population shift was found following irradiation of NIR laser. This result clearly indicates the system could kill cancer cells *via* apoptosis.

To clarify the differences in photo-induced cytotoxicity against cancer cells, the cellular uptake of Che6P-UCNPs was evaluated by flow cytometry. After 24 h of incubation, Colon26 cells treated with Che6P-UCNPs (Che6, 100 μg mL^{-1}) were analysed (Fig. 3b). There were no significant differences in cellular uptake among Che6P-UCNPs systems, indicating that cellular uptake does not affect the differences in photo-induced cytotoxicity found in Che6P-UCNPs. Moreover, the cellular uptake amount of Che6P-UCNPs systems in Colon26 cells were around 5 times larger than that in L929 cells (Fig. S18†). For oxidative stress toward specific organelles, including mitochondria[21] and lysosome[22] enhances the cytotoxicity from PDT, a subcellular distribution of delivered Che6P-UCNPs was observed by confocal laser scanning microscope (CLSM) after 24 h of incubation with Che6P-UCNPs. In all the systems, fluorescence signals from chlorin e6 were detected within cells (Fig. 3c and S19†), and there were no significant differences in distribution among Che6P-UCNPs. In addition, fluorescence signals from chlorin e6 of hybrid liposomes were faint, indicating the deliverability of photosensitizer of hybrid liposomes were lower than that of Che6P-UCNPs system (Fig. 3c bottom panel). We further examined ROS generation capacity within cells using a commercially available fluorescent probe, DCFH-DA, for ROS detection.[23] ROS expression level in Colon26 cells treated with Che6P-0.54-UCNPs-100 with NIR-laser irradiation were 16 times larger than that without NIR-laser irradiation (Fig. S20†), indicating that the system can efficiently convert energy from NIR-laser into ROS even in cells.
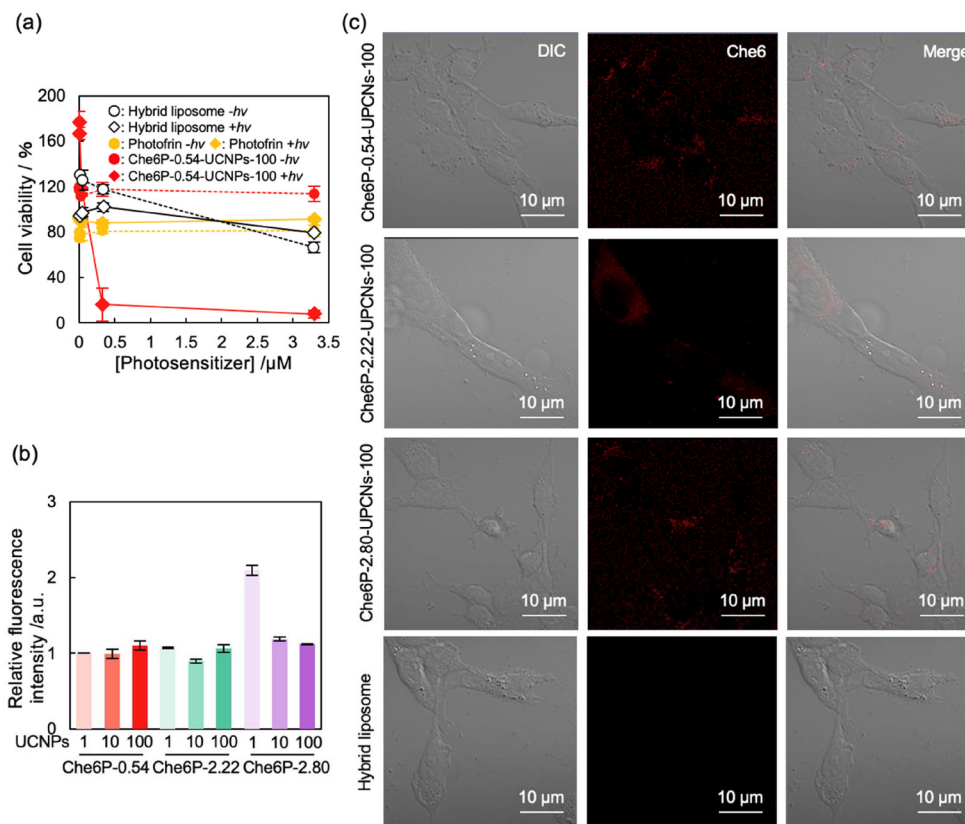
Fig. 3 Photodynamic activity against cancer cells. (a) Photo-induced cytotoxicity toward Colo26 cells. Colon26 cells were co-incubated with Che6P-0.54-UCNPs-100 (red), Photofrin (yellow), and hybrid liposomes (white) for 24 h. The cells were exposed to a 980 nm laser for 30 min (solid line, diamond symbol), and dark control was maintained in an incubator (dashed line, circle symbol). After additional 24 h, cell viability was estimated by WST-8 assay ($n = 3$). Data are present as mean $\pm$ standard deviation ($n = 3$). (b) Relative cellular uptake of Che6P-UCNPs. Colon26 cells were exposed to Che6P-UCNPs (polymer concentration, 0.1 mg mL^{-1}) for 24 h. The cells were analyzed by flow cytometry. Data are presented as mean $\pm$ standard deviation ($n = 3$). (c) Subcellular distribution of the delivered Che6P-UCNPs. Colon26 cells were exposed to Che6P-0.54-UCNPs-100 (polymer concentration, 0.1 mg mL^{-1}) for 24 h. The samples were observed by CLSM.

Photodynamic activity of hybrid nanoparticles toward spheroid

We demonstrated the potential applicability of Che6P-0.54-UCNPs-100 as a photosensitizer toward cancer spheroid, which is used as advanced tumor tissue model.[24] We used the cancer spheroid prepared with EZ sphere[25] after Colon26 cell spheroids grew up to 100 μm. The deliverability of Che6P-0.54-UCNPs-100 in cancer spheroids was investigated using CLSM. In case of Photofrin and hybrid liposomes, their fluorescence signals were faint (Fig. 4a and Fig. S21†). In contrast, stronger signals were three-dimensionally spread through the cancer spheroids (Fig. 4b). Che6P-0.54-UCNPs-100 could penetrate the center of spheroids compared to Photofrin. This capability to penetrate deeper tissues is preferable to induce cell death uniformly in tumor tissues.

The performance of photosensitizer was addressed by WST-8 assay. After 24 h of incubation with Che6P-0.54-UCNPs-100 or Photofrin (Che6P-0.54, 100 μg mL^{-1}; Che6, 3 μM : Photofrin, 3 μM), the treated spheroids were exposed to 980 nm laser for 30 min. After additional 24 or 48 h, cell viability was quantified by WST-8 assay. In case of Photofrin and

hybrid liposomes, photo-induced cytotoxicity was not induced toward Colon26 in the current condition (Fig. 4c). In contrast, 60% of colon cells were killed by 980 nm laser irradiation after 24 and 48 h of incubation. Spheroidal growth was examined *via* inhibition assay. After exposure to 980 nm laser, the volume of spheroids was significantly shrunk only when exposed to Che6P-0.54-UCNPs-100 (Fig. 4d). Regrowth was not observed during the period, and several spheroids collapsed at four days after laser ablation. In contrast, Photofrin and hybrid liposomes could not suppress spheroid growth even after NIR laser exposure; the concentration of porphyrin unit and Che6P-0.54-UCNPs-100 was the same. These results demonstrate that Che6P-UCNPs are potentially applicable as an NIR-activatable photosensitizer for cancer treatment in complex biological settings.

Photodynamic activity of hybrid nanoparticles *in vivo*

The photodynamic activity against tumor xenograft model mice was demonstrated. The estimation of peak in accumulation of photosensitizer toward tumor tissue is critical to maximize the therapeutic benefits from PDT. A pharmacoki-
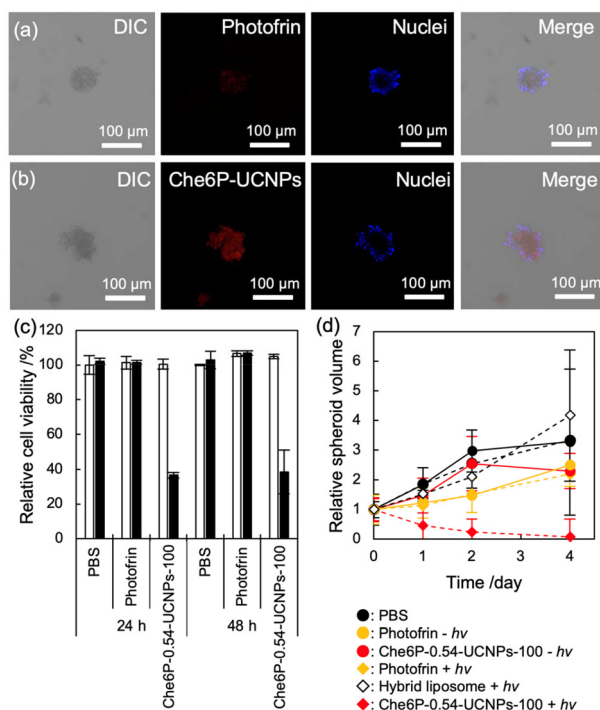
Fig. 4 Therapeutic efficacy of PDT using Che6P-UCNPs toward cancer spheroid. Distribution of the Photofrin (a) and Che6P-0.54-UCNPs-100 (b) in the Colon26 spheroid. Colon26 spheroid was exposed to Che6P-0.54-UCNPs-100 or Photofrin (Che6P-0.54-UCNPs-100, 0.1 mg mL^{-1} ([chlorin e6] = 3.25 μM); Photofrin, 3.25 μM) for 24 h. The cells were stained with Hoechst 33342. (c) Photodynamic activity toward Colon26 spheroid. Colon26 spheroids were co-incubated with Che6P-0.54-UCNPs-100 or Photofrin (Che6P-0.54-UCNPs-100, 0.1 mg mL^{-1} ([chlorin e6] = 3.25 μM); Photofrin, 3.25 μM) for 24 h. The spheroids were exposed to a 980 nm laser for 30 min. After 24 and 48 h, cell viability was measured by WST-8 assay. (White, without 980 nm laser irradiation; black, with 980 nm laser irradiation.) Data are presented as mean ± standard deviation (n = 3). (d) Spheroidal growth inhibition via PDT. Colon26 spheroids were co-incubated with Che6P-0.54-UCNPs-100 or Photofrin (Che6P-0.54-UCNPs-100, 100 μg mL^{-1} ([chlorin e6] = 3.25 μM); Photofrin, 3.25 μM) for 24 h. The spheroids were exposed to a 980 nm laser for 30 min (solid line). Non-irradiation controls are presented as a dashed line. The volume of spheroid was monitored at each time point (0, 1, 2, and 4 days). (Black, PBS; red, Che6P-0.52-UCNPs-100; yellow, Photofrin; white, hybrid liposome.) Data are presented as mean ± standard deviation (n = 10).

netic study was conducted for Che6P-0.54-UCNPs-100 and hybrid liposomes in tumor xenograft model mice by *in vivo* imaging system (NightOWL). Tumor xenograft model mice were established by transplantation of Colon26 cells to Balb/c mice (male, four weeks old, 18 g).[26] After 10 days of incubation (tumor volume reached approximately 80 mm^3), the mice received Che6P-0.54-UCNPs-100 (1 mg mL^{-1}, 200 μL) or hybrid liposomes intravenously. Severe side effects, including sudden death, diarrhea, and hair inversion, were not found in both systems in any mice, indicating that theses hybrid systems are nontoxic photosensitizer *in vivo*. The accumulation of the hybrid systems was visualized by NightOWL, and blood circulation was quantified by measuring the yttrium (Y) concentration using inductively

coupled plasma–atomic emission spectroscopy (ICP-AES).[27] Retention in blood stream of both systems were relatively short (Fig. 5a, closed circle) and the blood half-life time of Che6P-0.54-UCNPs-100 and hybrid liposomes were estimated to be 2.1 and 1 h, respectively. In addition, 75% of Che6P-0.54-UCNPs-100 and almost all the hybrid liposomes were excreted from blood at 24 h-post-injection. During the circulation, these hybrids can be accumulated in tumor tissues *via* EPR effect,[28] and fluorescence signals from Che6P-0.54-UCNPs-100 and hybrid liposomes in tumor tissues increased with time (Fig. 5b). As both Che6P-0.54-UCNPs-100 and hybrid liposomes accumulation in tumor tissues plateaued after reaching its peak at 6 h (Fig. 5a, open circle), NIR irradiation toward tumor tissues was done at 24 h-post-injection of the hybrid.

In addition, the Che6P-0.54-UCNPs-100 could deliver 20-fold chlorin e6 to tumor tissue than hybrid liposomes at the end point. At 24 h-post-injection, the organ distribution (tumor, heart, liver, spleen, lung, and kidney) of Che6P-0.54-UCNPs-100 and hybrid liposomes was evaluated *ex vivo* by measuring its fluorescence from chlorin e6, and the tumor showed the strongest fluorescence (Fig. S22†). The accumulation of the hybrid in each organ was quantified by measuring Y using ICP-AES. Y accumulation in each organ corresponded to the biodistribution results (Fig. 5c). To address the deliverability *in vivo*, the intratumoral distribution of delivered hybrid systems was observed; fluorescent signals from Che6P-0.54-UCNPs-100 were detected in both extracellular matrix and cytosol in highly dense tumor tissues (Fig. 5d). The systems could penetrate and spread three-dimensionally (Fig. S23†). These aspects of the current system are advantageous to induce efficient damages to cancer cells *via* oxidative stress by PDT. In contrast, fluorescence signals from hybrid liposomes were faint (Fig. S24†), and these results are comparable to the results in deliverability in spheroids.

Finally, the anti-tumor efficacy of Che6P-0.54-UCNPs-100 system in a murine colon carcinoma xenograft model was investigated. At 24 h-post incubation of Che6P-0.54-UCNPs-100, Photofrin[29] or hybrid liposomes, NIR laser was irradiated to the tumor tissue for 1 h (Fig. 5e). The controls, including saline, Photofrin without laser irradiation, hybrid liposomes without laser irradiation, Che6P-0.54-UCNPs-100 without laser irradiation, and Photofrin with light irradiation showed rapid tumor growth (1000 mm^3 at 17 days) (Fig. 5f and S25†). In contrast, NIR irradiation toward tumor xenograft model mice receiving Che6P-0.54-UCNPs-100 and hybrid liposomes could significantly suppress tumor growth (Fig. S25f and g†), and Che6P-0.54-UCNPs-100 exhibited the most excellent therapeutic efficacy among these groups. In addition, the average tumor volume was decreased to less than 1/400 of that in the non-irradiation control groups at 20 days after treatment, and photodynamic activity of Che6P-0.54-UCNPs-100 was 8 times higher than that of hybrid liposomes at 20 days after treatment. Moreover, there were no significant body weight loss in all groups during the experiment (Fig. 5g), suggesting that the system did not affect the long-term health of mice. Since a long-term exposure to photosensitizer and inorganic nanoparticle-based UCNPs can induce undesirable concerns,
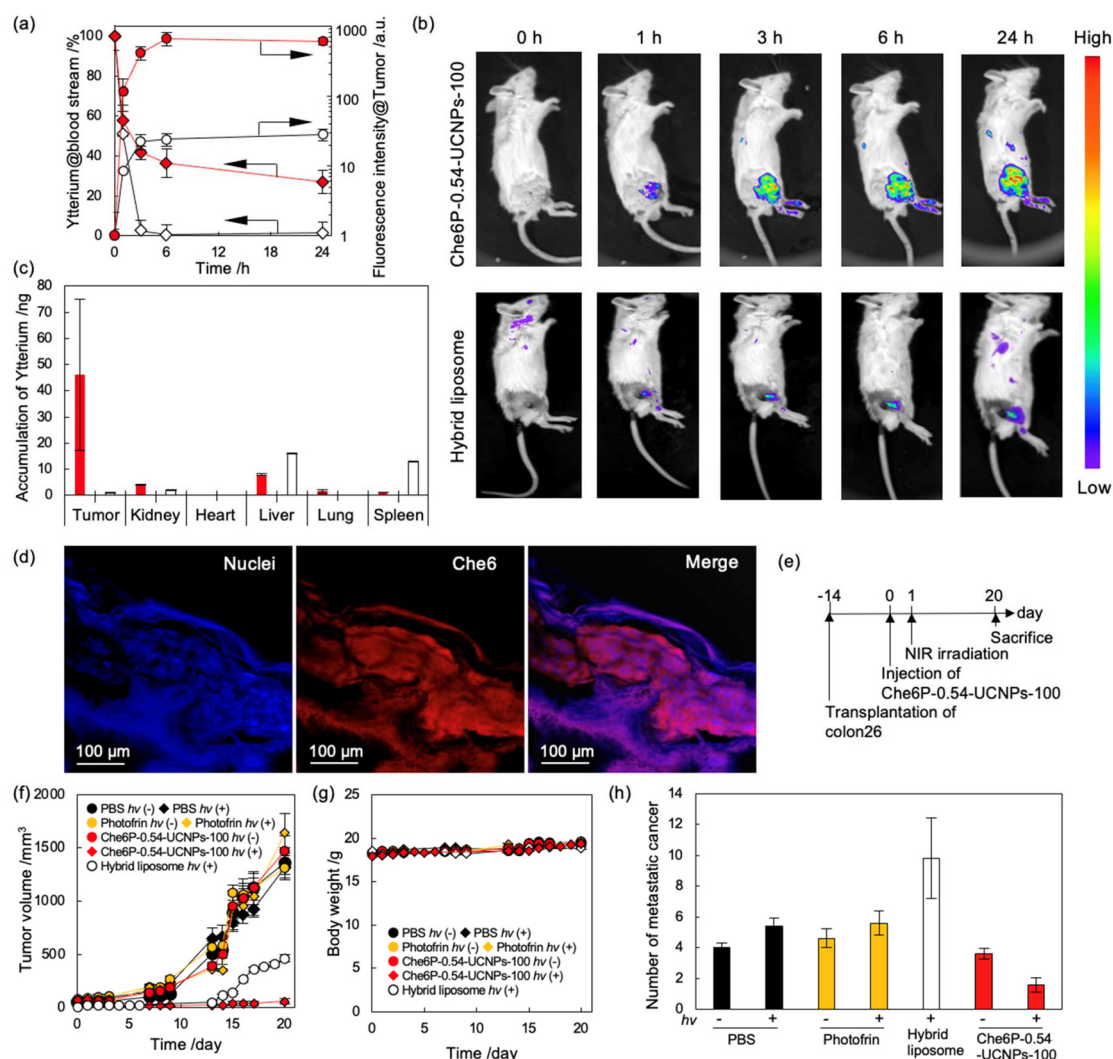
Fig. 5 Performance of Che6P-UCNPs as NIR-activatable photosensitizers. (a) Tumor accumulation and circulation in the blood stream of Che6P-0.54-UCNPs-100 in tumor xenograft model mice. Che6P-0.54-UCNPs-100 were administrated to tumor-xenograft model mice intravenously. At each time point (0, 1, 3, 6, and 24 h), the blood Y concentration was quantified by ICP-AES, and its accumulation in tumor tissues was quantified by measuring the fluorescence intensity, which was visualized by an *in vivo* imaging system. Data shown are mean $\pm$ SE ($n = 5$). (b) Biodistribution of Che6P-0.54-UCNPs-100. After the administration of Che6P-0.54-UCNPs-100, the mice were observed by an *in vivo* imaging system at each time point (0, 1, 3, 6, and 24 h). (c) Biodistribution of Che6P-0.54-UCNPs-100 and hybrid liposomes. After the administration, accumulation of yttrium using Che6P-0.54-UCNPs-100 (red) or hybrid liposomes (white) in each organ was quantified by ICP-AES. Data shown are mean $\pm$ SE ($n = 5$). (d) Intratumoral distribution of Che6P-0.54-UCNPs-100. After administration of Che6P-0.54-UCNPs-100, the tumor was isolated, and cellular nuclei were visualized by DAPI after permeabilization. (e) Time course for PDT using Che6P-0.54-UCNPs-100. (f) PDT activity of Che6P-0.54-UCNPs-100 under NIR-irradiation. Tumor xenograft model mice were treated with PBS (black), Photofrin (yellow), or Che6P-0.54-UCNPs-100 (red). Afterward the mice were irradiated with NIR laser (closed circle). Non-irradiation controls are shown in open circles. The tumor volume was calculated as (long axis) $\times$ (short axis)^2/2. Data shown are mean $\pm$ SE ($n = 5$). (g) Changes in body weight during the treatment. Data shown are mean $\pm$ SE ($n = 5$). (h) Inhibition of metastasis. At 20 days after NIR laser exposure, the lung was isolated, and metastasis was counted. Data shown are mean $\pm$ SE ($n = 5$).

including photosensitivity[30] and inflammatory[31] at worth oncologization, the photosensitizers and UCNPs should be excreted from the body after the treatment. To estimate the residual quantity of Che6P-0.54-UCNPs-100 at 20 days postinjection, the Y contents in each organ (heart, liver, spleen, lung, and kidney, and tumor) were measured using ICP-AES. As shown in Fig. S26,† the Y concentration in each organ of mice receiving Che6P-0.54-UCNPs and hybrid liposomes was

the same as that in the saline administered group, indicating that our hybrid systems were completely excreted from the body, so undesirable side effects caused by a long-term retention of the system can be avoided.

Because metastasis is the most fatal issue in cancer treatment due to malignancy and complexity,[32] the number of colonies formulated in the lungs by metastasis (Fig. 5h and S27†) was metastasis. Treatment with Che6P-0.54-UCNPs-100 under

NIR irradiation was twice as effective in metastasis inhibition compared to the control groups. Metastasis suppression should be obtained by efficient and uniform damages to cancer cells in tumor tissues, including cancer cells surrounding blood vessels, which is likely to metastasize, and cancer stem cells *via* PDT.

Conclusion

In conclusion, we developed a facile hybrid nanosystem comprising UCNPs and Che6P. Our system exhibited an excellent photodynamic activity *via* excellent energy transfer between UCNPs and Che6 molecules by controlling distances these two components and accessibility of dissolved oxygen to Che6 molecules under NIR laser irradiation, and the photodynamic activity from Che6P-UCNPs induced cell destruction *in vitro*. The hybrid system showed an excellent ability in generating singlet oxygen even in actively growing cancer spheroids. The efficient accumulation of Che6P-0.54-UCNPs-100 in tumor tissues in tumor xenograft mice resulted in NIR irradiation toward tumor xenograft model mice receiving Che6P-0.54-UCNPs-100, which could significantly suppress tumor growth. The average tumor volume was decreased to less than 1/400 of that in the control groups. In addition, photodynamic activity of Che6P-UCNPs *in vivo* was 8 times higher than that of hybrid liposomes which is employed as NIR activatable photosensitizer. Moreover, the systems could suppress cancer metastasis during the experiment. We believe that the hybrid systems are applicable as NIR-activatable photosensitizers for cancer therapy.

Author contributions

R. K. and A. I. designed this work. R. K., T. E., N. K., R. O., H. H., S. K., and K. Y. conducted all the work, N. T., and K. K. examined luminescent properties of upconversion nanoparticles. R. K., T. E., and A. I. wrote and revised the manuscript. All the authors approved the final manuscript.

Data availability

All relevant data are within the paper.

Conflicts of interest

There are no conflicts to declare.

Acknowledgements

References

1 I. Soerjomataram and F. Bray, *Nat. Rev. Clin. Oncol.*, 2021, **18**, 663–672.

2 K. Ganesh and J. Massague, *Nat. Med.*, 2021, **27**, 34–44.

3 H. Abrahamse and M. R. Hamblin, *Biochem. J.*, 2016, **473**, 347–364.

4 P. Mroz, A. Pawlak, M. Satti, H. Lee, T. Wharton, H. Gail, T. Sarna and M. R. Hamblin, *Free Radical Biol. Med.*, 2007, **43**, 711–719.

5 S. Yano, S. Hirohara, M. Obata, Y. Hagiya, S. Ogura, A. Ikeda, H. Kataoka, M. Tanaka and T. Joh, *J. Photochem. Photobiol., C*, 2011, **12**, 46–47.

6 Z. Sheng, D. Hu, M. Zheng, P. Zhao, H. Liu, D. Gao, P. Gong, G. Gao, P. Zhang, Y. Ma and L. Cai, *ACS Nano*, 2014, **8**, 12310–12322.

7 P. Agostinis, K. Berg, K. A. Cengel, T. H. Foster, A. W. Girotti, S. O. Gollnick, S. M. Hahn, M. R. Hamblin, A. Juzeniene, D. Kessel, M. Korbelik, J. Moan, P. Mroz, D. Nowis, J. Pitte, B. C. Wilson and J. Golab, *Ca-Cancer J. Clin.*, 2011, **61**, 250–281.

8 W. Sun, X. Zhao, J. Fan, J. Du and X. Peng, *Small*, 2019, **15**, 1804927.

9 C. A. Robertson, D. H. Evans and H. Abrahamse, *J. Photochem. Photobiol., B*, 2009, **96**, 1–8.

10 H. Y. Kim, M. Kang, Y. W. Choo, S. H. Go, S. P. Kwon, S. Y. Song, H. S. Sohn, J. Hong and B. S. Kim, *Nano Lett.*, 2019, **19**, 5185–5193.

11 M. R. Hamblin, *Dalton Trans.*, 2018, **47**, 8571–8580.

12 R. Kawasaki, R. Ohdake, R. K. Yamana, T. Eto, K. Sugikawa and A. Ikeda, *J. Mater. Chem. B*, 2021, **9**, 6357–6363.

13 S. Li, X. Wei, S. Li, C. Zhu and C. Wu, *Int. J. Nanomed.*, 2020, **15**, 9431–9445.

14 R. Kawasaki, Y. Sasaki, T. Nishimura, K. Katagiri, K. Morita, Y. Sekine, S. Sawada, S. Mukai and K. Akiyoshi, *Adv. Healthcare Mater.*, 2021, **10**, 2001988.

15 K. Katagiri, K. Ohta, K. Sako, K. Inumaru, K. Hayashi, Y. Sasaki and K. Akiyoshi, *ChemPlusChem*, 2014, **79**, 1631–1637.

16 S. K. Golombek, J. N. May, B. Theek, L. Appold, N. Drude, F. Kiessling and T. Lammers, *Adv. Drug Delivery Rev.*, 2018, **130**, 17–38.

17 P. Thanasekaran, C. H. Chu, S. B. Wang, K. Y. Chen, H. D. Gao, M. M. Lee, S. S. Sun, J. P. Li, J. Y. Chen, J. K. Chen, Y. H. Chang and H. M. Lee, *ACS Appl. Mater. Interfaces*, 2019, **11**, 84–95.

18 Z. Li, D. Wang, M. Xu, J. Wang, X. Hu, S. Anwar, A. C. Tedesco, P. C. Morias and H. Bi, *J. Mater. Chem. B*, 2020, **8**, 2598–2606.

19 R. Baskaran, J. Lee and S. G. Yang, *Biomater. Res.*, 2018, **22**, 25.

20 X. Zhang, R. Zhang, J. Huang, M. Luo, X. Chen, Y. Kang and J. Wu, *J. Mater. Chem. B*, 2019, **7**, 3575–3545.

21 D. R. Green and J. C. Reed, *Science*, 1998, **281**, 1309–1312.

22 N. Mizushima and M. Komatsu, *Cell*, 2011, **147**, 728–741.

23 W. A. Abd-Elraoof, A. A. Tayel, S. W. El-Far, O. M. W. Abukhatwah, A. M. Diab, O. M. Abonama, M. A. Assas and A. Abdella, *RSC Adv.*, 2023, **13**, 26001–26014.

24 A. S. Nunes, A. S. Barros, E. C. Costa, A. F. Moreira and I. J. Correia, *Biotechnol. Bioeng.*, 2019, **116**, 206–226.

25 F. Hirschhaeuser, H. Menne, C. Dittfeld, J. West, W. M. Klieser and L. A. K. Schughart, *J. Biotechnol.*, 2010, **148**, 3–15.

26 R. Kawasaki, Y. Sasaki, K. Katagiri, S. Mukai, S. Sawada and K. Akiyoshi, *Angew. Chem., Int. Ed.*, 2016, **55**, 11377–11381.

27 Z. Liu, B. Yang, B. Chen, M. He and B. Hu, *Analyst*, 2017, **142**, 197–205.

28 V. Torchilin, *Adv. Drug Delivery Rev.*, 2011, **63**, 131–135.

29 A. B. Ormond and H. S. Freeman, *Materials*, 2013, **6**, 817–840.

30 R. Saavedra, L. B. Rocha, J. M. Dabrowski and L. G. Arnaut, *ChemMedChem*, 2014, **9**, 390–398.

31 M. Firczuk, D. Nowis and J. Golab, *Photochem. Photobiol. Sci.*, 2011, **10**, 653.

32 D. Hanahan and R. A. Weinberg, *Cell*, 2011, **144**, 646–674.